Local characterization of collagen architecture and mechanical failure properties of fibrous plaque tissue of atherosclerotic human carotid arteries

Torun, Su Guvenir; Munoz, Pablo de Miguel; Crielaard, Hanneke; Verhagen, Hence J.M.; Kremers, Gert Jan; van der Steen, Antonius F.W.; Akyildiz, Ali C.

DOI
10.1016/j.actbio.2023.04.022

Publication date
2023

Document Version
Final published version

Published in
Acta Biomaterialia

Citation (APA)
Torun, S. G., Munoz, P. D. M., Crielaard, H., Verhagen, H. J. M., Kremers, G. J., van der Steen, A. F. W., & Akyildiz, A. C. (2023). Local characterization of collagen architecture and mechanical failure properties of fibrous plaque tissue of atherosclerotic human carotid arteries. *Acta Biomaterialia*, *164*, 293-302. https://doi.org/10.1016/j.actbio.2023.04.022

Acta Biomaterialia 164 (2023) 293–302

Contents lists available at ScienceDirect

Acta Biomaterialia

journal homepage: www.elsevier.com/locate/actbio

Full length article

Local characterization of collagen architecture and mechanical failure properties of fibrous plaque tissue of atherosclerotic human carotid arteries

Su Guvenir Torun[a], Pablo de Miguel Munoz[a,b], Hanneke Crielaard[a], Hence J.M. Verhagen[c], Gert-Jan Kremers[d], Antonius F.W. van der Steen[a,b], Ali C. Akyildiz[a,b,*]

[a] Department of Biomedical Engineering, Erasmus Medical Center, Rotterdam, the Netherlands
[b] Department of Biomechanical Engineering, Delft University of Technology, Delft, the Netherlands
[c] Department of Vascular Surgery, Erasmus Medical Center, Rotterdam, the Netherlands
[d] Erasmus Optical Imaging Center, Erasmus Medical Center, Rotterdam, the Netherlands

ARTICLE INFO

Article history:
Received 18 November 2022
Revised 5 April 2023
Accepted 13 April 2023
Available online 21 April 2023

Keywords:
Atherosclerosis
Digital image correlation
Mechanical testing
Plaque rupture
Second harmonic generation

ABSTRACT

Atherosclerotic plaque rupture in carotid arteries is a major cause of cerebrovascular events. Plaque rupture is the mechanical failure of the heterogeneous fibrous plaque tissue. Local characterization of the tissue's failure properties and the collagen architecture are of great importance to have insights in plaque rupture for clinical event prevention. Previous studies were limited to average rupture properties and global structural characterization, and did not provide the necessary local information. In this study, we assessed the local collagen architecture and failure properties of fibrous plaque tissue, by analyzing 30 tissue strips from 18 carotid plaques. Our study framework entailed second harmonic generation imaging for local collagen orientation and dispersion, and uniaxial tensile testing and digital image correlation for local tissue mechanics. The results showed that 87% of the imaged locations had collagen orientation close to the circumferential direction (0°) of the artery, and substantial dispersion locally. All regions combined, median [Q1:Q3] of the predominant angle measurements was -2° [-16°:16°]. The stretch ratio measurements clearly demonstrated a nonuniform stretch ratio distribution in the tissue under uniaxial loading. The rupture initiation regions had significantly higher stretch ratios (1.26 [1.15-1.40]) than the tissue average stretch ratio (1.11 [1.10-1.16]). No significant difference in collagen direction and dispersion was identified between the rupture regions and the rest of the tissue. The presented study forms an initial step towards gaining better insights into the characterization of local structural and mechanical fingerprints of fibrous plaque tissue in order to aid improved assessment of plaque rupture risk.

Statement of significance

Plaque rupture risk assessment, critical to prevent cardiovascular events, requires knowledge on local failure properties and structure of collagenous plaque tissue. Our current knowledge is unfortunately limited to tissue's overall ultimate failure properties with scarce information on collagen architecture. In this study, local failure properties and collagen architecture of fibrous plaque tissue were obtained. We found predominant circumferential alignment of collagen fibers with substantial local dispersion. The tissue showed nonuniform stretch distribution under uniaxial tensile loading, with high stretches at rupture spots. This study highlights the significance of local mechanical and structural assessment for better insights into plaque rupture and the potential use of local stretches as risk marker for plaque rupture for patient-specific clinical applications.

* Corresponding author.
E-mail address: a.akyildiz@erasmusmc.nl (A.C. Akyildiz).

https://doi.org/10.1016/j.actbio.2023.04.022

1. Introduction

Atherosclerotic plaque rupture in carotid arteries is the trigger of many ischemic cerebrovascular events, such as ischemic stroke [1,2]. Carotid endarterectomy (CEA) is a commonly used surgery to prevent such clinical events. The patient selection for CEA is based on, besides some systemic factors (e.g., age, gender, cardiovascular event history), only one plaque-based measure, the degree of carotid artery stenosis [3]. However, degree of stenosis is shown to be a poor predictor of plaque rupture, hence only a fraction of the operated patients benefit from the CEA surgery [4]. Other factors, such as the plaque compositional characteristics were also found to be important indicators for such events. For this purpose American Heart Association (AHA) provided a guide for plaque classification [5,6], modified later by Virmani et al. [7]. According to this classification, rupture prone vulnerable plaques were identified as Type IV, thin cap fibroatheroma with a large lipid core [8]. However, the mentioned and some other vulnerable plaque characteristics [9,10] are not always associated with plaque rupture. This clearly indicates an urgent need for other patient-specific plaque-based measures that are predictive for plaque rupture.

From the biomechanics perspective, plaque rupture is the material failure of the fibrous plaque tissue, which, together with some other structural tissue components (i.e., necrotic lipid core, calcifications, healthy arterial wall layers), constitute the atherosclerotic plaque. To understand plaque rupture mechanics, unraveling the tissue's failure characteristic is of great importance. However, up until now only a few studies have been performed. While in some of these studies failure properties of the entire plaque was obtained by testing complete plaques with all components intact [11–13], in the recent studies tissue-specific characterization was pursued for fibrous plaque tissue, separated from the rest of the plaque [14,15]. Regardless of the tested tissue type (whole plaque or fibrous tissue), all studies so far focused on the ultimate failure characteristics. Although ultimate strength and stretch ratio measures can provide some insight for tissue's failure properties, it has been shown that the macroscopic structural failure in the highly heterogenous fibrous plaque tissue initiates much earlier than the ultimate failure point [15]. This implies that, rather than the assessment of the (average) tissue properties at ultimate failure point, the assessment of the failure properties locally at the failure initiation point is more relevant for having better insights into plaque rupture.

The material properties of biological tissues depend on the underlying tissue structure (microstructural components and their organization) [16]. Fibrous plaque tissue is a highly collagenous tissue [17,18]. It has been shown that in healthy arteries the fibrillar collagen is the main load bearing constituent and arterial wall's mechanical behavior, including the failure (rupture) properties, greatly depends on the organization of the collagen fibers [19–21]. Similarly, for the fibrous plaque tissue, the collagen architecture was suggested to dictate the tissue's failure properties [22]. Until now, only two studies investigated the collagen organization in atherosclerotic plaques. Akyildiz et al. assessed the collagen fiber organization in carotid plaques using ex-vivo diffusion tensor magnetic resonance imaging (DT-MRI). They reported that the collagen fibers lay mainly on the circumferential-longitudinal plane with negligible radial orientation [23]. More recently, Johnston et al. examined the fiber orientation in fibrous caps of carotid plaques with small angle light scattering (SALS), which provides higher resolution information [14]. They observed that some caps had a global (average) collagen orientation in the circumferential direction whereas the others in the longitudinal direction. Despite the great contribution of these studies on the overall collagen fiber organization in plaques, there is still a gap in our current knowledge on the local collagen organization characteristics and the link of it to the failure properties in fibrous plaque tissue.

In this study, we investigated the local structural and mechanical failure properties of the fibrous plaque tissue collected from atherosclerotic human carotid arteries. To this end, we used second harmonic generation multiphoton microscopy imaging (SHG) for tissue's local collagen architecture assessment. Compared to other techniques (e.g. as histology [24,25], SALS [14], DTI [23,26,27]) used for collagen architecture imaging in biological tissues, SHG has various advantages, including high resolution [28], faster acquisition, and no need of tissue preparation [26,29,30]. The local failure properties of the fibrous plaque tissue were acquired from mechanical tissue testing and digital image correlation (DIC). To the best of our knowledge, our study is the first to report both local structural and mechanical failure characteristics of fibrous plaque tissue, and to provide their correlation locally at rupture initiation, which is highly crucial for better understanding and predicting atherosclerotic plaque rupture.

2. Materials and methods

2.1. Sample collection and preparation

Eighteen human CEA samples, obtained from at least 70% stenosed arteries, were collected according to the European Guidelines [3] at Erasmus Medical Center in Rotterdam. Following the tissue collection, the samples were snap-frozen in plastic vials submerged into liquid nitrogen, and were stored at -80°C. The use of the CEA samples in this study was approved by the Medical Ethics Committee of Erasmus Medical Center in Rotterdam in compliance with the declaration of Helsinki. An informed consent from the patient was obtained for each sample used in this study.

In order to visualize the calcified regions prior to tissue preparation, all collected CEA samples (Fig. 1A) were scanned with a micro computed tomography (micro-CT) scanner (Quantum GX 2, Perkin Elmer, USA). The voltage and current of the scanner were 90 kV and 88 mA, respectively. Each scan took approximately 4 minutes. Following the micro-CT imaging, the CEA sample's 3-D anatomy were reconstructed by using the 3-D Slicer (v 4.11) [31] (Fig. 1B). From the micro-CT data, the calcified regions in samples were identified and rectangular shaped tissue strips (Fig. 1C) were prepared from the non-calcified fibrous tissue regions, that likely resembled type IV or type V lesions [5–8]. The sample size was aimed to be large enough with a width to length ratio <1, as advised by Mulvihill et al. [32], for the suitability for uniaxial tensile testing. The length dimension of the strips was in the circumferential direction of the artery.

2.2. Imaging and quantification of the fibrillar collagen architecture

Following the sample preparation, the tissue strips were submerged into a phosphate buffered saline (PBS) solution in a glass petri dish. To avoid any movement of the tissue strips during the microscopy imaging, the strips were fixated with the use of surgical needles to silicone rubber (Elastosil E41, Wacker, Germany) blocks (width:2cm, length:2cm and height:1cm) that had been cured on the glass petri dish bottom (Fig. 2A). A multiphoton microscope (TCS SP5 Confocal, Leica, Germany) with a Chameleon Ultra multiphoton laser (710-1040nm) (Coherent, USA) was used to visualize the fibrillar collagen architecture based on SHG (Fig. 2B). Prior to the imaging, by using the bright field mode, a quick scan ($\sim$2 mins) of the tissue strips were performed to place a grid, composed of tiles with the size of approximately 739×739 µm, for guiding the coordinates of the imaged locations. A multiphoton laser with an excitation wavelength of 880 nmFig and a non-descanned detector of 430 to 450 nm were used to obtain

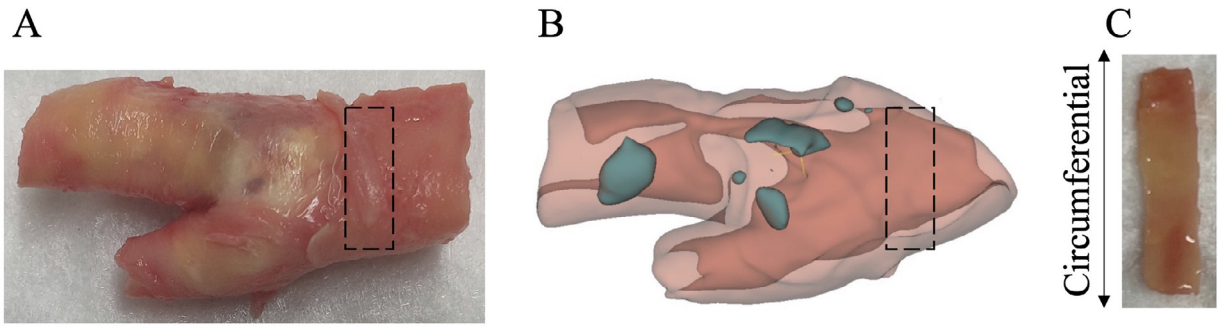

Fig. 1. Fibrous plaque tissue sample preparation. (A) Carotid plaque sample collected in an endarterectomy (CEA) surgery. (B) 3-D plaque anatomy reconstructed from the micro computed tomography (micro-CT) scan of the CEA sample, used to locate the calcifications within the tissue. (Calcifications are in turquoise color.) (C) A rectangular shaped fibrous tissue strips, with the long axis aligned in circumferential direction, obtained from a non-calcified region of the CEA sample. (For interpretation of the references to color in this figure legend, the reader is referred to the web version of this article.)

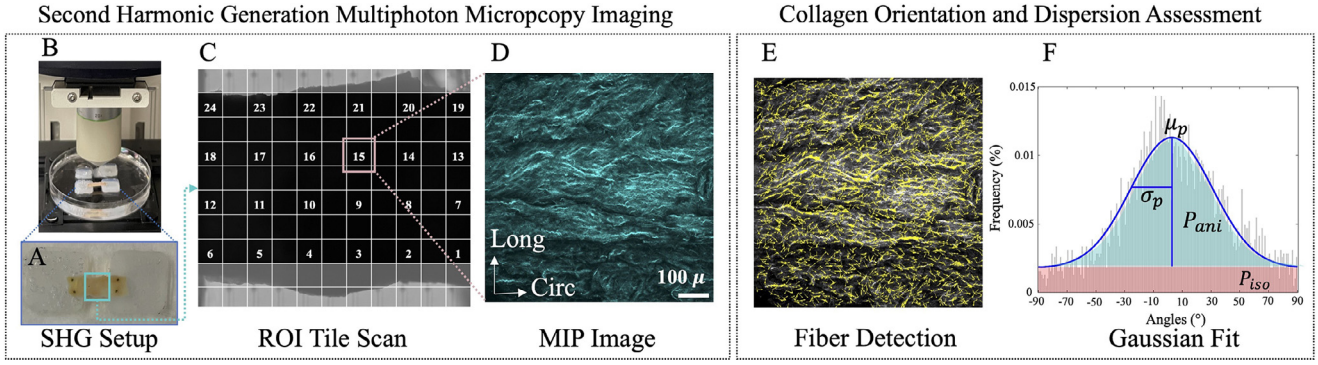

Fig. 2. The pipeline of quantitative structural imaging of fibrillar collagen organization. (A) Test strip fixated with surgical needles to a silicone rubber cured on the glass petri dish filled with PBS. (B) Strip under the microscope. (C) ROI Tile scan per each tile performed by SHG. The imaging was performed by skipping one to two tiles between each defined tile in both circumferential and longitudinal directions (D) MIP image obtained from image stack. (E) Fiber detection by using the Fiblab Software for obtaining the histogram of detected collagen fibers. (D) Fitting Gaussian Distribution to the collagen fiber histogram to obtain μ_p, σ_p, P_{iso} and P_{ani} parameters. (SHG: Second Harmonic Generation Multiphoton Microscopy Imaging, ROI: Region of Interest, MIP: Maximum Intensity Projection, μ_p: the pre-dominant angle, σ_p: standard deviation, P_{iso}: isotropic fraction, P_{ani}: anisotropic fraction)

structural collagen images (512×512 pixels, final resolution 1.44 μm/pixel) in every selected tile. Images were obtained at every 3 μm depth up to an approximately of 150 μm depth from the luminal surface. The scanning time per each tile took ~10 mins on average. Depending on the sample size, the imaging was performed by skipping one to two tiles between each defined tile in both circumferential and longitudinal directions (Fig. 2C). This selection of tile subsets was in order to avoid long scanning times.

For the data analysis, the maximum intensity projection (MIP) image of each scanned tile was obtained (Fig. 2D). The MIP images were analyzed using Fiblab [33] to extract the orientation histogram of the detected collagen fibers (Fig. 2E). By fitting Gaussian Distribution to the histogram, the pre-dominant angle (μ_p), and two dispersion parameters, the standard deviation (σ_p) and the anisotropic fraction (P_{ani}), were obtained per each imaged tile (Fig. 2F). μ_p was defined as the peak of the fit and σ_p as the standard deviation of the distribution. In the histogram, the area below the baseline frequency is defined as the isotropic fraction (P_{iso}) and the one above as the anisotropic fraction (P_{ani}). Please note that $P_{ani} + P_{iso} = 1$ [33]. Further details of the imaging can be found in elsewhere [34].

2.3. Mechanical testing

Immediately after the SHG, the tissue strips were prepared for mechanical testing. First, a speckle pattern was applied on the luminal surface of the strips, by using an airbrush filled with black tissue dye (24113-2, Polysciences Inc., Ott Scientific) to enable local tissue deformation measurements with a DIC analysis. Subsequently, the strips were placed into a custom-built uniaxial tensile testing setup. The setup consisted of two clamps (one stationary and one moving), a heating bath filled with 37°C PBS solution, a 10 N load cell (LCMFD-10N, Omega Engineering, USA), a linear actuator (EACM2E10AZAK, Oriental Motor, Japan), a ring-shaped light source and a 5.3 Megapixels CMOS Camera (PL-D725, Pixelink, USA) (Fig. 3A). In order to minimize tissue slippage in the clamps, sandpapers (P180, Conrad Electronic Benelux B.V., The Netherlands) were glued to the inner face of the clamps and a torque screwdriver (Garant, Germany) was used to apply 0.2 Nm on clamp screws.

At the beginning of the tensile testing, a pre-load of 0.05N was applied to remove the tissue slack and have a flat strip surface. Then, the strip thickness was measured by 3-D scanning the strip with an ultrasound system (Vevo 3100, FUJIFILM, Visual Sonics Inc., Canada) using a 21 MHz central frequency 2-D linear transducer (MX250) (resolution in the tissue thickness direction = 75 μm). Afterwards, the strips were preconditioned 10-times under uniaxial tensile conditions up to 10% of the gauge-length (GL), which was defined as the distance between the two clamps. Following the preconditioning, the strips were stretched with a constant speed of 0.05 mm/s until complete failure. The strips were video-recorded by the high-resolution camera with 5 frames/s during the tests for subsequent DIC analysis (Fig. 3B).

2.4. Global ultimate failure and local failure assessments

The force recordings and the GL based displacement measurements were used to calculate the commonly used global ultimate

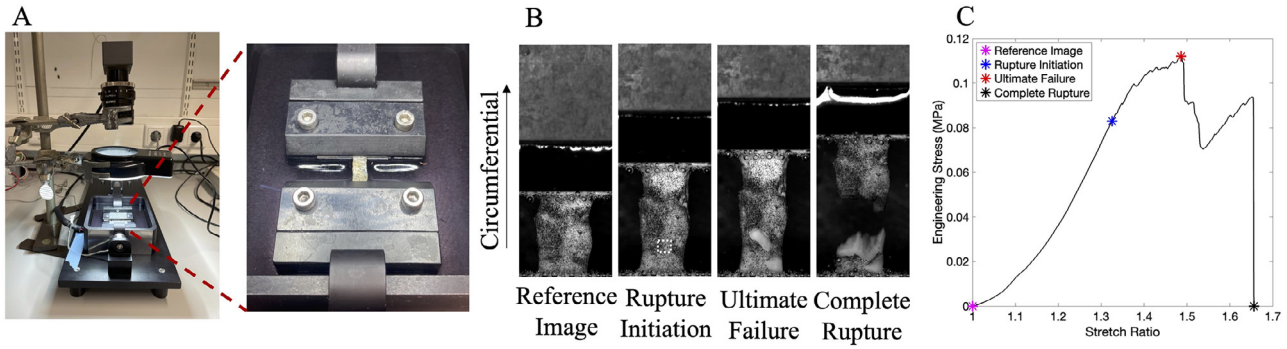

Fig. 3. Uniaxial tensile testing until tissue failure. (A) The custom-built tensile testing setup. (B) Various stages during the uniaxial tensile testing. (C) The stages marked on the tensile stress-stretch ratio curve.

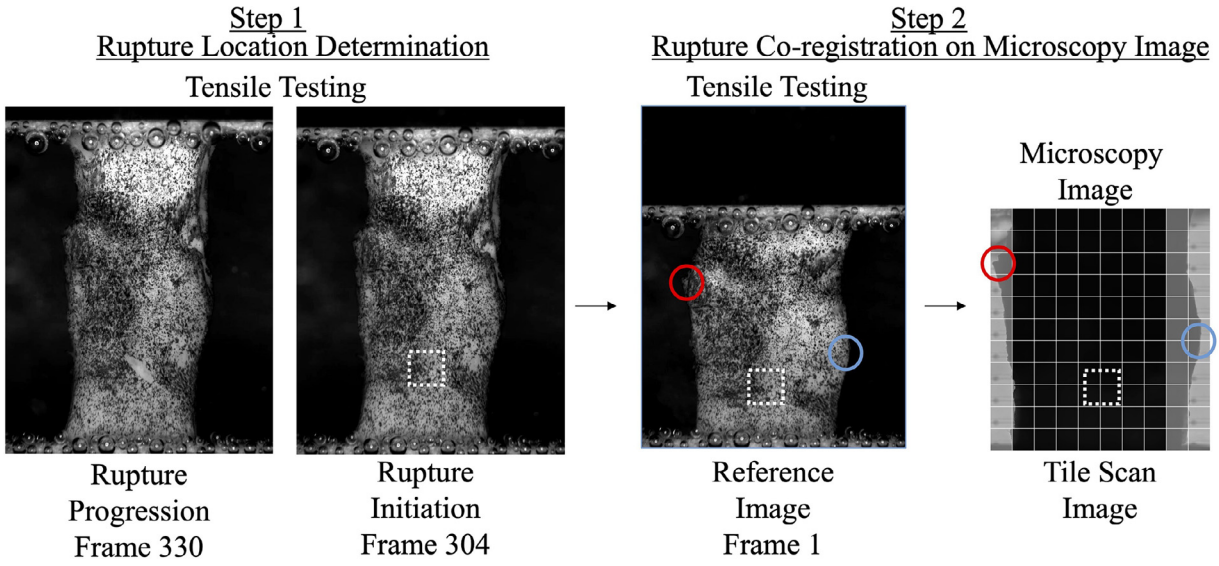

Fig. 4. The procedure for rupture-specific (Frame 330) structural information acquisition. Step 1: Visual identification of rupture initiation (Frame 304) and the rupture location both on the rupture initiation frame (Frame 304) and on the reference frame *(Frame 1)*. Step 2: Rupture region co-registered to the microscopy image using the anatomical landmarks (marked in red and blue circles).

failure stress and stretch ratio (the peak of the stress-stretch ratio curve) (Fig. 3C). For stress calculations, the thickness measurements from the ultrasound scans were used. Engineering stress is reported in the rest of the paper as the stress measure, and the stretch ratio as the deformation measure.

For the local failure assessment, DIC analyses of the video recordings of the strips were performed with Ncorr Open-Source 2-D DIC Software (version 1.2) [35]. A subset radius of 30 pixels and a spacing of 3 pixels were used for DIC. DIC-derived maximum stretch ratio at the rupture initiation location were reported for local failure assessment. Rupture initiation was detected by visual inspection. Moreover, average stretch ratio within the strip's region of interest (ROI) was calculated. The ROI was defined as the tissue area between the two clamps excluding the strip regions that are within ~1 mm distance from each clamp. These regions were excluded to avoid any noisy data in the DIC measurements due to the presence of air bubbles that accumulated near the clamps.

2.5. Fiber architecture determination at rupture initiation

Following the mechanical testing, the rupture location was determined by careful visual examination of the high-resolution camera (5.3 MP CMOS, 5 frames/s) recordings (Step 1 in Fig. 4). After the rupture region was identified on the rupture initiation frame (Step 1, Frame 304 in Fig. 4), the same location was identified on the reference image frame (Step 2, Frame 1, Fig. 4), with the aid of the distinct local pattern of the speckles in this region. Then, the recognition of the rupture region on the microscopy image was performed manually by using the natural anatomical landmarks of the specimen shape, such as the curved segments of the edges. A few of such landmarks are indicated (red and blue circles) for the representative case in Fig. 4 (Step 2). Once the co-registration of the reference camera frame to the microscopy image was performed successfully, the fiber orientation and dispersion information in the rupture region were obtained from the microscopy image.

2.6. Statistical methods

The average stretch ratio from the ROI of the strips and the maximum stretch ratio at the rupture initiation location were compared by using non-parametric Wilcoxon signed rank test for a statistical significance. In addition, the local structural parameters μ_p, σ_p and P_{ani} between the rupture initiation region and the non-rupture regions were compared by using a Linear Mixed Model. The Linear Mixed Model approach was selected for the statistical analysis as the regions were not independent (i.e., some regions were from the same strip), which was implemented in the model by identifying the individual tissue strip numbers as random factor. All analyses were performed with SPSS (IBM SPSS 27 Software,

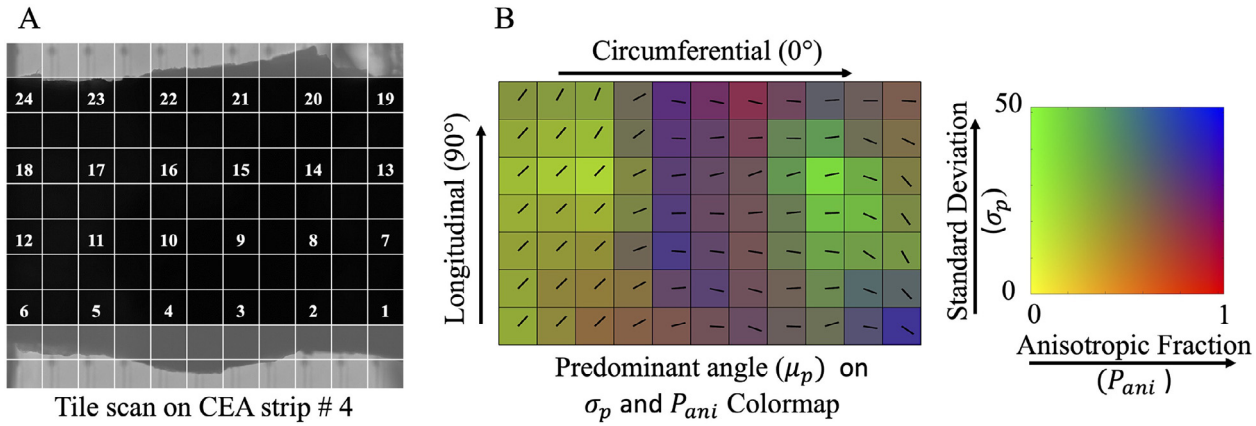

Fig. 5. (A) Tile scan applied on a representative tissue strip (#4) during the second harmonic generation multiphoton microscopy imaging (SHG) (Note that only the numbered tiles were imaged), (B) the map of the predominant angle (μ_p) (represented by black lines), and the standard deviation (σ_p) and the anisotropic fraction (P_{ani}) (both represented by the colormap) for this representative tissue strip (Please note that the values for the unnumbered tiles were obtained from interpolation, only for illustrative purposes here.). (For interpretation of the references to color in this figure legend, the reader is referred to the web version of this article.)

Armonk, New York) and a p-value < 0.05 was considered significant.

3. Results

3.1. Collagen fiber organization

From 18 CEA samples, 30 rectangular-shaped fibrous plaque tissue strips were obtained. On all tissue strips, SHG was performed successfully, and the collagen fiber organization parameters (i.e., μ_p, σ_p and P_{ani}) were measured locally. A representative case (tissue strip #4) is shown in Fig. 5(A). The local μ_p (black lines) and, σ_p and P_{ani} (background color for both) measurements on the strip are illustrated in Fig. 5(B). For this representative strip, 17 (71%) of the 24 scanned tiles showed a predominant circumferential alignment (i.e., -45°<μ_p<45°, circumferential direction = 0°). The median [Q1:Q3] value was 8° [-9°:44°] for μ_p, 25° [22°:30°] for σ_p, and 0.57 [0.36:0.69] for P_{ani}.

For the entire strip set (n = 30), 17 (± 5) tiles per strip were imaged on average. The distributions of μ_p, σ_p, and P_{ani} per tissue strip is demonstrated in Fig. 6. In overall, for 87% of the 497 tiles imaged, μ_p was between -45° and 45°, indicating an alignment closer to circumferential direction rather than longitudinal. All tiles from all strips combined (n = 497), the median [Q1:Q3] was -2° [-16°:16°] for μ_p, 23° [19°:29°] for σ_p, and 0.49 [0.38:0.62] for P_{ani}.

3.2. Gauge length based ultimate failure characteristics

Of the 30 tissue strips, 16 were tested mechanically. The remaining 14 strips could not be used for mechanical tissue characterization due to existing structural damages prior testing (identified in high-resolution camera images). The mean (± SD) thickness was 1.1 (± 0.4) mm, the mean width was 3.3 (± 1.1) mm, and the mean length was 5.9 (± 2.6) mm, for the mechanically tested 16 strips. (Please note that the length dimension was along the circumferential direction of the artery and the width along the axial direction.) The width to length (W/L) ratio for all test strips was < 1 (mean ± SD of 0.6 ± 0.2), where the average relative standard deviation for the width of the strips was 6.4% and the one for the thickness was 15.2%. Sample specific dimension could be found in the supplementary material (Supplementary Table I). The tensile stress-stretch ratio curves of all strips until the ultimate failure are demonstrated in Fig. 7(A). In all 16 tested strips, non-linear stiffening behavior was observed. Five of the strips had the final complete rupture in the central region (i.e., at least ~1 mm away from the clamps) and 11 strips in a clamp region (within ~1 mm from the clamps) (a representative case per each category is shown with their corresponding stress-stretch ratio curves in Supplementary Material Fig. 1). The ultimate tensile stress for the central rupture cases ranged between 0.12 and 0.36 MPa with a median of 0.26 MPa, and for the clamp rupture cases between 0.16 and 1.01 MPa with a median of 0.33 MPa (Fig. 7(B)). The associated ultimate stretch ratio values for the central rupture cases ranged between 1.16 and 1.49 with a median of 1.33, whereas for the clamp rupture cases it ranged between 1.20 and 1.64 with a median of 1.42 (Fig. 7(C)). Although one would expect the opposite trend from the theoretical viewpoint, interestingly both ultimate tensile stress and stretch ratio values for the clamp rupture group were slightly higher than the central rupture group; however with no statistical significance between the two groups.

3.3. Rupture initiation site: DIC-derived failure stretch ratio

Of the 16 strips that were mechanically tested, nine strips had rupture initiation in the central region. These nine strips included the five strips with a final rupture in the central region and four others, which had the final complete rupture in a clamp region, but the rupture initiation in the central region. The latter group of four strips was added to the analysis as the rupture initiation was in the central region and the DIC measurements were still reliable. For these nine strips, the stretch ratio at the rupture initiation site could be assessed with DIC analysis, whereas for the other seven strips with the rupture initiation at a clamp, bubbles accumulated at the clamps prevented DIC analysis at the rupture initiation site. DIC-derived tensile stretch ratio results at the rupture initiation timepoint on a CEA strip (#13) with the rupture initiation in the central region is shown in Fig. 8(A). For the strip, the tensile stretch ratio distribution was nonuniform and ranged up to 1.20 with a median of 1.10. The rupture initiation site had a stretch ratio of 1.17. The nonuniform stretch ratio distribution was observed for all nine strips with the range up to 1.63 with a median of 1.12, where the ROI-average stretch ratios varied from 1.07 to 1.18 with a median of 1.11 (Fig. 8(B)). The max tensile stretch ratio at the rupture initiation sites ranged from 1.10 to 1.47 with a median of 1.26, and were statistically significantly higher than the ROI-average stretch ratios (Fig. 8(B)).

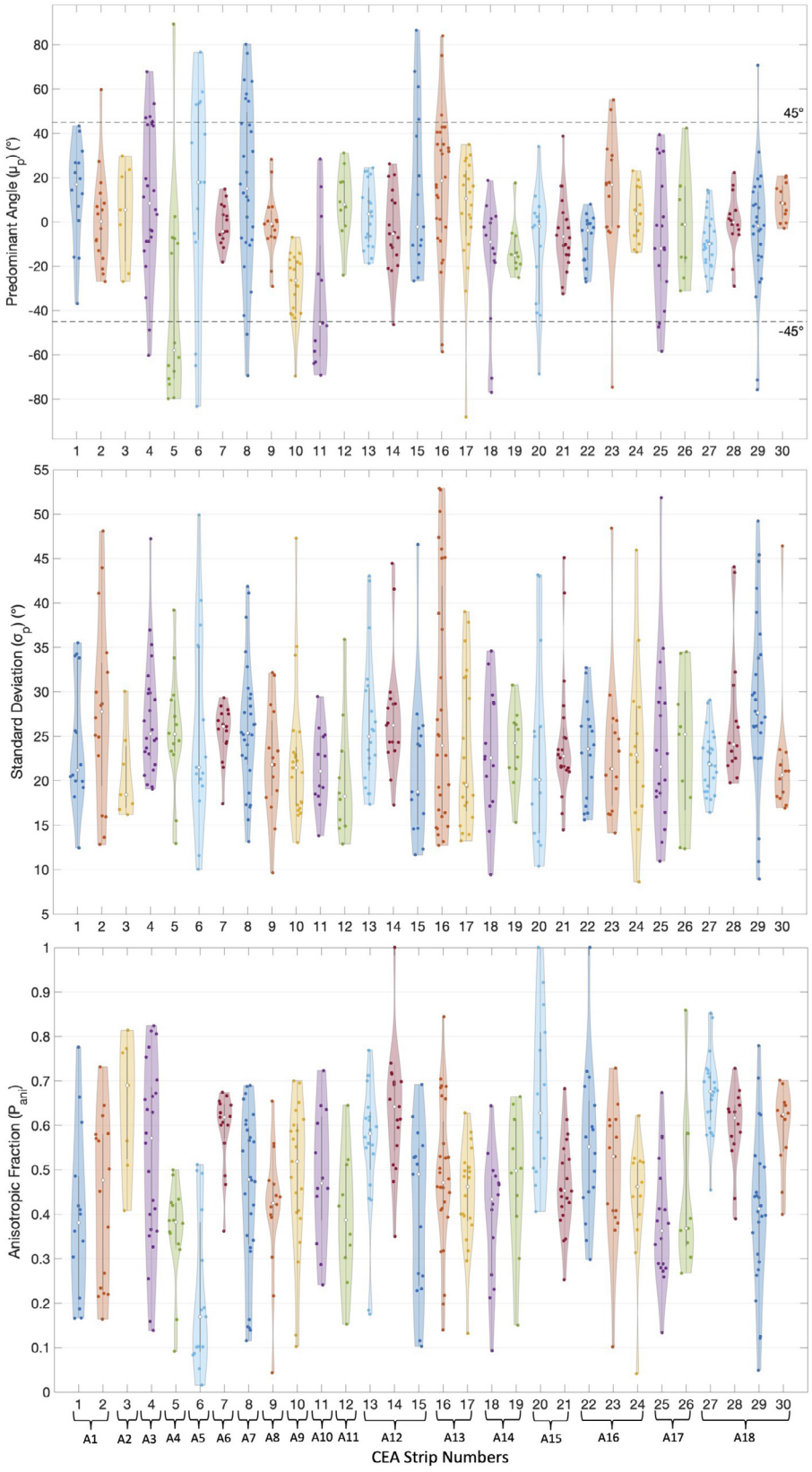

Fig. 6. The predominant angle (μ_p), standard deviation (σ_p) and anisotropic fraction (P_{ani}) measurements per tissue strip. Each solid dot indicates the value measured in a tile. "A" indicates the artery number.

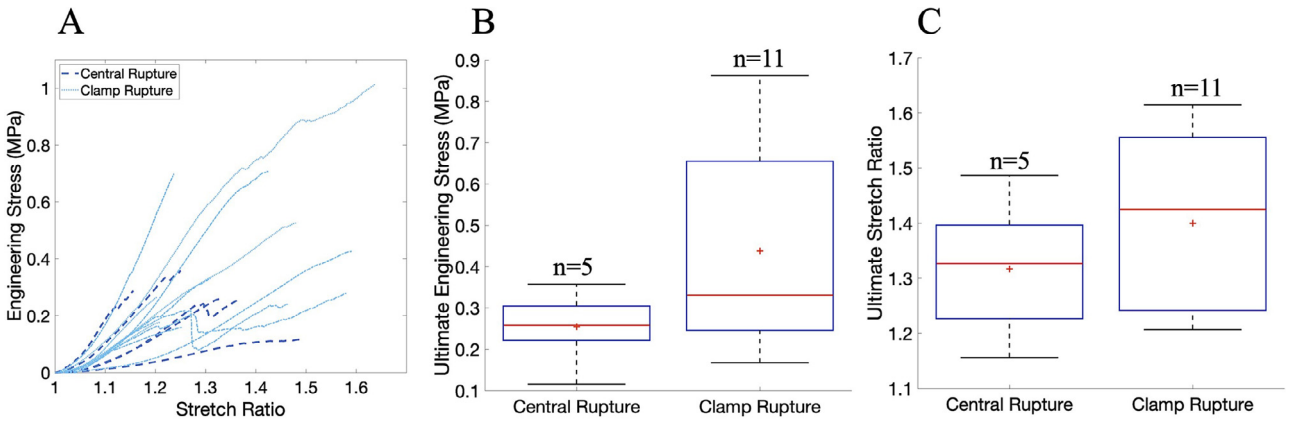

Fig. 7. Tensile stress-stretch ratio curves of the mechanically tested tissue strips ($n = 16$). (A) The ultimate stress (B) and stretch ratio (C) of the strips with a rupture in the central ($n = 5$) or clamp region ($n = 11$).

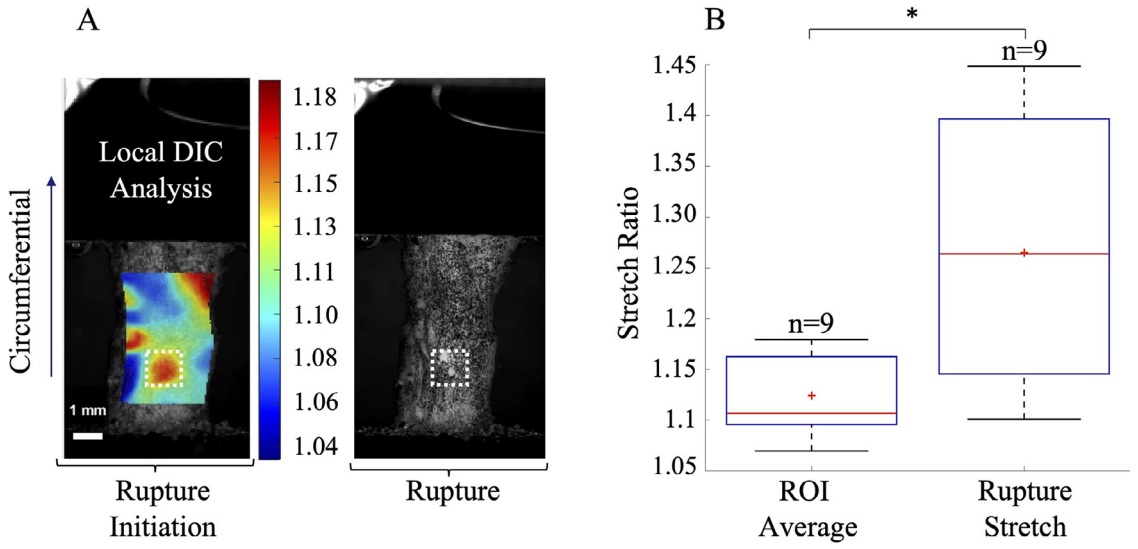

Fig. 8. (A) DIC-derived tensile stretch ratio results of a CEA sample (#13) with central rupture initiation. The rupture initiation region is marked with the white square. (B) DIC-derived average tensile stretch ratio and maximum stretch ratio in the rupture initiation region for nine strips (* Significant difference according to the non-parametric Wilcoxon Signed Rank test with a p-value<0.05).

3.4. Rupture initiation site: collagen fiber organization

The structural information of tissue strips with center region rupture were analyzed to compare the collagen fiber organization in the rupture regions with the ones in the non-ruptured regions. Comparison of the nine rupture regions to the 138 non-ruptured regions (here the regions refer to the tiles of the SHG) from nine tissue strips with a central rupture in terms of μ_p, σ_p and P_{ani} are shown in (Fig. 9). For the rupture regions, the median [Q1:Q3] was -4° [-15°:28°] for the μ_p, 26° [19°:30°] for the σ_p, and 0.53 [0.43:0.61] for the P_{ani}. Meanwhile, the non-ruptured regions had median [Q1:Q3] of 5° [-11°:22°] for the μ_p, 23° [19°:29°] for the σ_p, and 0.51 [0.39:0.64] for the P_{ani}. No statistical significance in these structural measures were found between the ruptured and non-ruptured regions.

4. Discussion

In this study, we examined the local mechanical failure and structural properties of atherosclerotic plaque fibrous tissue, in order to gain fundamental insights for atherosclerotic plaque rupture. Special attention was put on rupture initiation as this is more relevant than the ultimate failure analysis for understanding the rupture mechanics of the heterogenous plaque. This required high resolution, local assessment of failure and structural properties, which we achieved with DIC and SHG assessments.

Our local predominant angle measurements demonstrate that the local collagen fiber orientation in plaque fibrous tissue usually closer to the circumferential direction rather than the longitudinal direction, although there is some deviation from the exact circumferential direction. The structural organization in plaques was also investigated previously by Johnston et al. [14] and Akyildiz et al. [23]. Whereas the former group's SALS measurements demonstrated slightly less circumferential alignment of collagen fibers in fibrous caps (40%) than we did in our current study, the latter one identified with DTI a predominant circumferential alignment in CEA samples, similar to our findings. The main loading due to the *in-vivo* cyclic pressure in the arteries is in the circumferential direction. As also suggested for the healthy arterial wall layers by Timmins et al. [36], the collagen fibers have a crucial role in the overall load-bearing task in biological tissues. The predominant circumferential alignment of collagen fibers in plaque fibrous tissue supposedly helps this function during intraluminal pressurization of the artery [37].

Besides the predominant angle, we also assessed local dispersion of the collagen fibers, through two parameters, σ_p and P_{ani}.

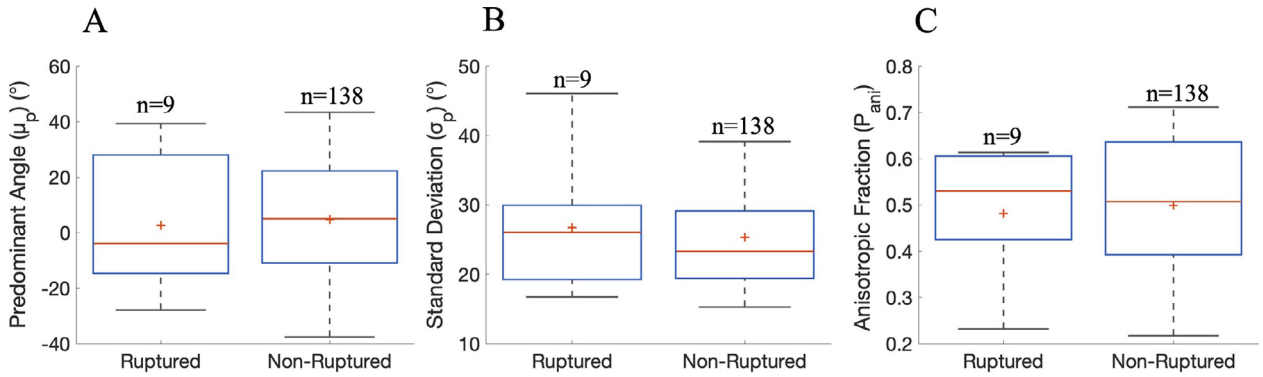

Fig. 9. The predominant angle (μ_p), standard deviation (σ_p) and anisotropic fraction (P_{ani}) of ruptured ($n = 9$) and non-ruptured ($n = 138$) regions of the nine strips with central rupture.

Fiber dispersion is an important structural feature for fibrous tissues as it impacts the tissue's (anisotropic) mechanical behavior [38]. We observed substantial inter- and intra-strip variation for both dispersion parameters. Similar to our findings, Johnston et al. in carotid plaques [14], and Douglas et al. in coronary plaques [25] observed intra- and inter-sample dispersion of collagen fibers. These findings indicate that not all collagen fibers are perfectly oriented in the predominant direction. This may serve the purpose to aid the redistribution of the stress and stretch ratio more uniformly within the plaque where the complex geometry of atherosclerotic plaque cause highly nonuniform stress and stretch ratio distribution [39,40].

To examine any local structural difference between rupture initiation region and the rest of the tissue, we compared the ruptured and non-ruptured tiles. Our analyses did not demonstrate any statistically significant difference in μ_p, σ_p and P_{ani} between the two groups. However, it is important to emphasize that these structural parameters were obtained in the unloaded state of the fibrous tissue strips before the mechanical testing. During the mechanical loading the collagen fibers may undergo affine or non-affine deformation [41], leading to reorientation of the fibers and change in the fiber dispersion. Future studies can examine this by combining structural imaging with mechanical testing, as suggested by Jett et al. [42], that combined polarized spatial frequency domain imaging system with a biaxial mechanical testing device.

The fibrous plaque tissue demonstrated non-linear stiffening behavior prior rupture under uniaxial loading, also shown by others previously for fibrous plaque tissue and entire plaques [11–15,43]. With regards to rupture characterization, although our main focus was on rupture initiation, we also assessed the ultimate rupture properties to compare our findings to the previously reported ones. By employing the commonly used GL-based assessment, we identified median [Q1:Q3] ultimate tensile strength for the strips with central rupture. Our results (0.26 [0.22-0.30] MPa) are within the range of the values reported previously for fibrous plaque tissue, where Johnston et al. [14] measured slightly higher (0.59 [0.40-1.41] MPa, ultimate engineering stress for the strips with predominant circumferential fiber alignment) and Teng et al. [15] slightly lower (0.16 [0.07-0.26] MPa, ultimate Cauchy stress) values than ours. For the ultimate stretch ratio, Johnston et al. [14] observed a median value of 1.09 [1.05-1.12] (for the strips with predominant circumferential fiber alignment) and Teng et al. [15] a median value of 1.18 [1.10-1.27]. Our results (1.33 [1.23-1.40]) are higher than these two studies, yet the measured range (1.16 -1.49) is comparable what Teng et al. [15] reported (1.03-1.47). However, it should be noted that these compared studies used different approaches for strain measurements, such as DIC or marker tracing. In our study, the global deformation measurements were based on gauge length measurements. Hence, the global strain result differences could be partly due to the differences in strain measurement techniques. In addition, both studies investigated fibrous plaque tissues from cap regions whereas our study was not limited to the specimens from the cap region. Both our results and the ones from the work of Johnston et al. [14] demonstrate regional variance in the structural features of fibrous plaque tissue, even within a tested specimen. Future studies are warranted to research any possible structural differences between the plaque caps and the non-cap plaque regions, beyond the already demonstrated local differences.

Our DIC analyses showed large local variation in stretch ratio values. This behavior, in our opinion, is not surprising considering the heterogenous structure of the fibrous tissue [14,44], and clearly indicates the necessity of local stretch ratio measurements for accurate failure characterization of the fibrous plaque tissue, rather than average stretch ratio measurements for the entire tissue strip [45], obtained from e.g. traditional GL-based assessment. Moreover, we observed that the rupture initiation happened always much earlier than the ultimate rupture, the former being more relevant for gaining better insights into plaque rupture. Another important finding of the current study is that the rupture initiation sites showed always high local stretch ratios. This indicates the possibility of local stretch ratio to be used as an imaging for rupture risk assessment marker in atherosclerotic plaques. In coronary arteries, local stretch ratio measurements can be achieved with intravascular imaging techniques based on ultrasound [46] and optical coherence tomography [47]. For carotid arteries, extracorporeal ultrasound can provide such stretch ratio measurements [48].

There are some limitations associated with this study. (1) The SHG was advantageous in several aspects; however, the imaging depth was limited to ~150 μm. Our (unreported) analysis showed similar structural fiber organization at different depths within this imaging depth of SHG. Further research is warranted to check if the collagen architecture differs in deeper segments. Yet, we expect the findings of our study on structure and mechanical behavior relation to hold since both strain measurements and rupture events were captured on the luminal surface. (2) DIC provided the assessment of the luminal surface deformation, not any subsurface deformation. The latter can be quantified by the combination of optical coherence tomography and digital volume correlation [49]. Yet, we think that the luminal surface deformation quantification provides the necessary information for characterization of the rupture on the luminal surface. (3) The mechanical testing was performed in the circumferential direction. Although the main in-vivo loading is in this direction, a more comprehensive analysis of the anisotropic behavior can be performed by testing the tissue in the other directions under uniaxial tensile loading or biaxial tensile testing con-

ditions. Moreover, our tests were quasi-static and did not include any dynamic component, that is present in vivo plaque loading, for instance, due to the pulsatility of the blood pressure. The influence of such dynamic effects on plaque rupture is still unclear as the biological tissues structurally adapt and remodel depending on the loading exerted on them. (4) Collagen amount (content) may be another important structural feature. However, this study was not designed to obtain collagen content information as Johnston et al. [14] and Davis et al. [50] demonstrated that the collagen content in fibrous cap samples did not have a significant influence on tissue's strength. (5) Besides the local stretch ratios obtained in this study, the information of local stresses, mainly at the rupture initiation regions is of importance to obtain a comprehensive analysis on the complex rupture process. However, this requires local stiffness knowledge. This can be potentially obtained by inverse finite element modeling approach, which was previously used for the stiffness assessment of the individual plaque components [51,52], and warrants future studies. (6) The W/L ratio obtained in this study is in accordance with the study of Mulvihill et al. [32], where the specimens with a W/L ratio < 1 were deemed suitable for uniaxial tensile testing. As advised in their study, due to the challenges in acquiring human plaques samples and for the risks of affecting the mechanical properties of during small dimension sample preparation, tissue strips with W/L ratio <1 were included in this study with possible minor strains (strain in the direction orthogonal to the loading direction) associated $< 12\%$. (7) The local thickness affect both the local stress and strain measures. Further research is warranted for the assessment of local thickness at rupture regions.

5. Conclusion

Atherosclerotic plaque rupture is a local mechanical failure of the fibrous plaque tissue. Local structural and mechanical characterization of the heterogeneous atherosclerotic fibrous tissue, especially in the rupture initiation location is crucial for having better insights in plaque rupture. To the best of our knowledge, this study is the first one that provided local structural and mechanical characteristics of the fibrous plaque tissue, and their correlations at the rupture and non-ruptured regions. Our structural findings suggest an overall collagen orientation that is close to circumferential direction, with substantial fiber dispersion locally. Under uniaxial tensile testing conditions in the circumferential direction, the fibrous tissue demonstrated a clear non-uniform stretch distribution. The local stretches at the rupture initiation sites were statistically significantly higher than the rest of the tissue. This further demonstrates the importance of local tissue characterization for better insights into the mechanics of plaque rupture and a potential use of stretch as a rupture risk marker.

Declaration of Competing Interest

The authors declare that they have no known competing financial interests or personal relationships that could have appeared to influence the work reported in this paper.

Funding

This project received funding from European Commission's Horizon 2020 under the Marie Skłodowska-Curie grant agreement # 749283.

Ethical Approval

The CEA sample usage was approved by the Medical Ethics Committee of Erasmus Medical Center in Rotterdam and an informed consent was obtained for all the samples used in this study.

Acknowledgements

The authors would like to thank to Robert Beurskens, Yanto Ridwan, Aikaterini Tziotziou, Dr. Jolanda Wentzel and Prof. Aad van der Lugt for their support to this project.

Supplementary materials

Supplementary material associated with this article can be found, in the online version, at doi:10.1016/j.actbio.2023.04.022.

References

[1] S. Carr, A. Farb, W.H. Pearce, R. Virmani, J.S.T. Yao, Atherosclerotic plaque rupture in symptomatic carotid artery stenosis, J. Vasc. Surg. 23 (1996) 755–766, doi:10.1016/S0741-5214(96)70237-9.

[2] Yuan Chun, Zhang Shao-xiong, Nayak L. Polissar, Echelard Denise, Ortiz Geraldo, Joseph W. Davis, Ellington Elizabeth, Marina S. Ferguson, Thomas S. Hatsukami, Identification of fibrous cap rupture with magnetic resonance imaging is highly associated with recent transient ischemic attack or stroke, Circulation 105 (2002) 181–185, doi:10.1161/hc0202.102121.

[3] L.H. Bonati, S. Kakkos, J. Berkefeld, G.J. de Borst, R. Bulbulia, A. Halliday, I. van Herzeele, I. Koncar, D.J. McCabe, A. Lal, J.-B. Ricco, P. Ringleb, M. Taylor-Rowan, H.-H. Eckstein, European Stroke Organisation guideline on endarterectomy and stenting for carotid artery stenosis, Eur Stroke J 6 (2021) I–XLVII, doi:10.1177/23969873211012121.

[4] P. Rothwell, C. Warlow, Prediction of benefit from carotid endar terectomy in individual patients: a risk-modelling study, Lancet North Am. Ed. 353 (1999) 2105–2110, doi:10.1016/S0140-6736(98)11415-0.

[5] H.C. Stary, A.B. Chandler, S. Glagov, J.R. Guyton, W. Insull, M.E. Rosenfeld, S.A. Schaffer, C.J. Schwartz, W.D. Wagner, R.W. Wissler, A definition of initial, fatty streak, and intermediate lesions of atherosclerosis. A report from the Committee on Vascular Lesions of the Council on Arteriosclerosis, American Heart Association, Circulation 89 (1994) 2462–2478, doi:10.1161/01.cir.89.5.2462.

[6] H.C. Stary, A.B. Chandler, R.E. Dinsmore, V. Fuster, S. Glagov, W. Insull, M.E. Rosenfeld, C.J. Schwartz, W.D. Wagner, R.W. Wissler, A definition of advanced types of atherosclerotic lesions and a histological classification of atherosclerosis, Circulation 92 (1995) 1355–1374, doi:10.1161/01.CIR.92.5.1355.

[7] R. Virmani, F.D. Kolodgie, A.P. Burke, A. Farb, S.M. Schwartz, Lessons from sudden coronary death, arteriosclerosis, thrombosis, and vascular biology. 20 (2000) 1262–1275. https://doi.org/10.1161/01.ATV.20.5.1262.

[8] A. van Veelen, N.M.R. van der Sangen, J.P.S. Henriques, B.E.P.M. Claessen, Identification and treatment of the vulnerable coronary plaque, Rapid Commun. Mass Spectrom. 23 (2022) 39, doi:10.31083/j.rcm2301039.

[9] M. Naghavi, P. Libby, E. Falk, S.W. Casscells, S. Litovsky, J. Rumberger, J.J. Badimon, C. Stefanadis, P. Moreno, G. Pasterkamp, Z. Fayad, P.H. Stone, S. Waxman, P. Raggi, M. Madjid, A. Zarrabi, A. Burke, C. Yuan, P.J. Fitzgerald, D.S. Siscovick, C.L. de Korte, M. Aikawa, K.E. Juhani Airaksinen, G. Assmann, C.R. Becker, J.H. Chesebro, A. Farb, Z.S. Galis, C. Jackson, I.-K. Jang, W. Koenig, R.A. Lodder, K. March, J. Demirovic, M. Navab, S.G. Priori, M.D. Rekhter, R. Bahr, S.M. Grundy, R. Mehran, A. Colombo, E. Boerwinkle, C. Ballantyne, W. Insull, R.S. Schwartz, R. Vogel, P.W. Serruys, G.K. Hansson, D.P. Faxon, S. Kaul, H. Drexler, P. Greenland, J.E. Muller, R. Virmani, P.M. Ridker, D.P. Zipes, P.K. Shah, J.T. Willerson, From vulnerable plaque to vulnerable patient: a call for new definitions and risk assessment strategies: Part I, Circulation 108 (2003) 1664–1672, doi:10.1161/01.CIR.0000087480.94275.97.

[10] M. Naghavi, P. Libby, E. Falk, W. Casscells, S. Litovsky, J. Rumberger, J.J. Badimon, C. Stefanadis, P. Moreno, G. Pasterkamp, Z. Fayad, P. Stone, S. Waxman, P. Raggi, M. Madjid, A. Zarrabi, A. Burke, C. Yuan, P. Fitzgerald, D. Siscovick, C. de Korte, M. Aikawa, K.E. Juhani Airaksinen, G. Assmann, C. Becker, J. Chesebro, A. Farb, Z. Galis, C. Jackson, I.-K. Jang, W. Koenig, R. Lodder, K. March, J. Demirovic, M. Navab, S. Priori, M. Rekhter, R. Bahr, S. Grundy, R. Mehran, A. Colombo, E. Boerwinkle, C. Ballantyne, W. Insull Jr, R. Schwartz, R. Vogel, P. Serruys, G. Hansson, D. Faxon, S. Kaul, H. Drexler, P. Greenland, J. Muller, R. Virmani, P. Ridker, D. Zipes, P. Shah, J. Willerson, From vulnerable plaque to vulnerable patient: a call for new definitions and risk assessment strategies: Part II, Circulation (Baltimore) 108 (2003) 1772–1778, doi:10.1161/01.CIR.0000087481.55887.C9.

[11] E.M. Cunnane, J.J.E. Mulvihill, H.E. Barrett, M.M. Hennessy, E.G. Kavanagh, M.T. Walsh, Mechanical properties and composition of carotid and femoral atherosclerotic plaques: a comparative study, J. Biomech. 49 (2016) 3697–3704, doi:10.1016/j.jbiomech.2016.09.036.

[12] M.G. Lawlor, M.R. O'Donnell, B.M. O'Connell, M.T. Walsh, Experimental determination of circumferential properties of fresh carotid artery plaques, J. Biomech. 44 (2011) 1709–1715, doi:10.1016/j.jbiomech.2011.03.033.

[13] J.J. Mulvihill, E.M. Cunnane, S.M. McHugh, E.G. Kavanagh, S.R. Walsh, M.T. Walsh, Mechanical, biological and structural characterization of in vitro ruptured human carotid plaque tissue, Acta Biomater. 9 (2013) 9027–9035, doi:10.1016/j.actbio.2013.07.012.

[14] R.D. Johnston, R.T. Gaul, C. Lally, An investigation into the critical role of fibre orientation in the ultimate tensile strength and stiffness of human carotid

plaque caps, Acta Biomater. 124 (2021) 291–300, doi:10.1016/j.actbio.2021.02.008.
[15] Z. Teng, J. Feng, Y. Zhang, M.P.F. Sutcliffe, Y. Huang, A.J. Brown, Z. Jing, Q. Lu, J.H. Gillard, A uni-extension study on the ultimate material strength and extreme extensibility of atherosclerotic tissue in human carotid plaques, J. Biomech. 48 (2015) 3859–3867, doi:10.1016/j.jbiomech.2015.09.037.
[16] P. Fratzl, Collagen: structure and mechanics, an introduction, in: P. Fratzl (Ed.), Collagen: Structure and Mechanics, Springer US, Boston, MA, 2008, pp. 1–13, doi:10.1007/978-0-387-73906-9_1.
[17] M. Rekhter, Collagen synthesis in atherosclerosis: too much and not enough, Cardiovasc. Res. 41 (1999) 376–384, doi:10.1016/S0008-6363(98)00321-6.
[18] E.B. Smith, The influence of age and atherosclerosis on the chemistry of aortic intima: Part 2. Collagen and mucopolysaccharides, J. Atheroscler. Res. 5 (1965) 241–248, doi:10.1016/S0368-1319(65)80065-5.
[19] G.A. Holzapfel, Collagen in arterial walls: biomechanical aspects, in: P. Fratzl (Ed.), Collagen: Structure and Mechanics, Springer US, Boston, MA, 2008, pp. 285–324, doi:10.1007/978-0-387-73906-9_11.
[20] J.D. Humphrey, Cardiovascular Solid Mechanics: Cells, Tissues, and Organs, Springer Science & Business Media, 2002.
[21] S. Sugita, T. Matsumoto, Local distribution of collagen fibers determines crack initiation site and its propagation direction during aortic rupture, Biomech. Model. Mechanobiol. 17 (2018) 577–587, doi:10.1007/s10237-017-0979-2.
[22] G.A. Holzapfel, J.J. Mulvihill, E.M. Cunnane, M.T. Walsh, Computational approaches for analyzing the mechanics of atherosclerotic plaques: a review, J. Biomech. 47 (2014) 859–869, doi:10.1016/j.jbiomech.2014.01.011.
[23] A.C. Akyildiz, C.-K. Chai, C.W.J. Oomens, A. van der Lugt, F.P.T. Baaijens, G.J. Strijkers, F.J.H. Gijsen, 3D Fiber orientation in atherosclerotic carotid plaques, J. Struct. Biol. 200 (2017) 28–35, doi:10.1016/j.jsb.2017.08.003.
[24] C. Pagiatakis, R. Galaz, J.-C. Tardif, R. Mongrain, A comparison between the principal stress direction and collagen fiber orientation in coronary atherosclerotic plaque fibrous caps, Med. Biol. Eng. Comput. 53 (2015) 545–555, doi:10.1007/s11517-015-1257-z.
[25] G.R. Douglas, A.J. Brown, J.H. Gillard, M.R. Bennett, M.P.F. Sutcliffe, Z. Teng, Impact of fiber structure on the material stability and rupture mechanisms of coronary atherosclerotic plaques, Ann. Biomed. Eng. 45 (2017) 1462–1474, doi:10.1007/s10439-017-1827-3.
[26] S. Ghazanfari, A. Driessen-Mol, G.J. Strijkers, F.M.W. Kanters, F.P.T. Baaijens, C.V.C. Bouten, A comparative analysis of the collagen architecture in the carotid artery: Second harmonic generation versus diffusion tensor imaging, Biochem. Biophys. Res. Commun. 426 (2012) 54–58, doi:10.1016/j.bbrc.2012.08.031.
[27] V. Flamini, C. Kerskens, C. Simms, C. Lally, Fibre orientation of fresh and frozen porcine aorta determined non-invasively using diffusion tensor imaging, Med. Eng. Phys. 35 (2013) 765–776, doi:10.1016/j.medengphy.2012.08.008.
[28] C.R. Esquibel, K.D. Wendt, H.C. Lee, J. Gaire, A. Shoffstall, M.E. Urdaneta, J.V. Chacko, S.K. Brodnick, K.J. Otto, J.R. Capadona, J.C. Williams, K.W. Eliceiri, Second harmonic generation imaging of collagen in chronically implantable electrodes in brain tissue, Front Neurosci 14 (2020) https://www.frontiersin.org/articles/10.3389/fnins.2020.00095. (Accessed 12 August 2022).
[29] A.J. Schriefl, H. Wolinski, P. Regitnig, S.D. Kohlwein, G.A. Holzapfel, An automated approach for three-dimensional quantification of fibrillar structures in optically cleared soft biological tissues, J. R. Soc. Interface 10 (2013) 20120760, doi:10.1098/rsif.2012.0760.
[30] S.-W. Teng, H.-Y. Tan, J.-L. Peng, H.-H. Lin, K.H. Kim, W. Lo, Y. Sun, W.-C. Lin, S.-J. Lin, S.-H. Jee, P.T.C. So, C.-Y. Dong, Multiphoton autofluorescence and second-harmonic generation imaging of the ex vivo porcine eye, Invest. Ophthalmol. Vis. Sci. 47 (2006) 1216–1224, doi:10.1167/iovs.04-1520.
[31] A. Fedorov, R. Beichel, J. Kalpathy-Cramer, J. Finet, J.-C. Fillion-Robin, S. Pujol, C. Bauer, D. Jennings, F. Fennessy, M. Sonka, J. Buatti, S. Aylward, J.V. Miller, S. Pieper, R. Kikinis, 3D Slicer as an image computing platform for the quantitative imaging network, Magn. Reson. Imaging 30 (2012) 1323–1341, doi:10.1016/j.mri.2012.05.001.
[32] J.J. Mulvihill, M.T. Walsh, On the mechanical behaviour of carotid artery plaques: the influence of curve-fitting experimental data on numerical model results, Biomech. Model. Mechanobiol. 12 (2013) 975–985, doi:10.1007/s10237-012-0457-9.
[33] E.E. van Haaften, T.B. Wissing, M.C.M. Rutten, J.A. Bulsink, K. Gashi, M.A.J. van Kelle, A.I.P.M. Smits, C.V.C. Bouten, N.A. Kurniawan, Decoupling the effect of shear stress and stretch on tissue growth and remodeling in a vascular graft, Tissue Eng. Part C 24 (2018) 418–429, doi:10.1089/ten.tec.2018.0104.
[34] H. Crielaard, S. Guvenir Torun, T.B. Wissing, P. de Miguel Muñoz, G.-J. Kremers, F.J.H. Gijsen, K. Van Der Heiden, A.C. Akyildiz, A method to study the correlation between local collagen structure and mechanical properties of atherosclerotic plaque fibrous tissue, J. Vis. Exp. (2022) e64334, doi:10.3791/64334.
[35] J. Blaber, B. Adair, A. Antoniou, Ncorr: Open-Source 2D digital image correlation matlab software, Exp. Mech. 55 (2015) 1105–1122, doi:10.1007/s11340-015-0009-1.
[36] L.H. Timmins, Q. Wu, A.T. Yeh, J.E. Moore, S.E. Greenwald, Structural inhomogeneity and fiber orientation in the inner arterial media, Am. J. Physiol.-Heart Circulat. Physiol. 298 (2010) H1537–H1545, doi:10.1152/ajpheart.00891.2009.
[37] J.M. Clark, S. Glagov, Transmural organization of the arterial media. The lamellar unit revisited, Arteriosclerosis 5 (1985) 19–34, doi:10.1161/01.atv.5.1.19.
[38] G.A. Holzapfel, R.W. Ogden, S. Sherifova, On fibre dispersion modelling of soft biological tissues: a review, Proc. R. Soc. A 475 (2019) 20180736, doi:10.1098/rspa.2018.0736.
[39] A.C. Akyildiz, L. Speelman, H. van Brummelen, M.A. Gutiérrez, R. Virmani, A. van der Lugt, A.F. van der Steen, J.J. Wentzel, F.J. Gijsen, Effects of intima stiffness and plaque morphology on peak cap stress, Biomed. Eng. Online 10 (2011) 25, doi:10.1186/1475-925X-10-25.
[40] A.C. Akyildiz, L. Speelman, H.A. Nieuwstadt, H. van Brummelen, R. Virmani, A. van der Lugt, A.F.W. van der Steen, J.J. Wentzel, F.J.H. Gijsen, The effects of plaque morphology and material properties on peak cap stress in human coronary arteries, Comput. Meth. Biomech. Biomed. Eng. 19 (2016) 771–779, doi:10.1080/10255842.2015.1062091.
[41] C. Morin, S. Avril, C. Hellmich, Non-affine fiber kinematics in arterial mechanics: a continuum micromechanical investigation, Z. Angew. Math. Mech. 98 (2018) 2101–2121, doi:10.1002/zamm.201700360.
[42] S.V. Jett, L.T. Hudson, R. Baumwart, B.N. Bohnstedt, A. Mir, H.M. Burkhart, G.A. Holzapfel, Y. Wu, C.-H. Lee, Integration of polarized spatial frequency domain imaging (pSFDI) with a biaxial mechanical testing system for quantification of load-dependent collagen architecture in soft collagenous tissues, Acta Biomater. 102 (2020) 149–168, doi:10.1016/j.actbio.2019.11.028.
[43] Z. Teng, D. Tang, J. Zheng, P.K. Woodard, A.H. Hoffman, An experimental study on the ultimate strength of the adventitia and media of human atherosclerotic carotid arteries in circumferential and axial directions, J. Biomech. 42 (2009) 2535–2539, doi:10.1016/j.jbiomech.2009.07.009.
[44] E. Maher, A. Creane, S. Sultan, N. Hynes, C. Lally, D.J. Kelly, Tensile and compressive properties of fresh human carotid atherosclerotic plaques, J. Biomech. 42 (2009) 2760–2767, doi:10.1016/j.jbiomech.2009.07.032.
[45] B.L. O'Reilly, N. Hynes, S. Sultan, P.E. McHugh, J.P. McGarry, An experimental and computational investigation of the material behaviour of discrete homogenous iliofemoral and carotid atherosclerotic plaque constituents, J. Biomech. 106 (2020) 109801, doi:10.1016/j.jbiomech.2020.109801.
[46] C.L. De Korte, A.F.W. van der Steen, E.I. Céspedes, G. Pasterkamp, S.G. Carlier, F. Mastik, A.H. Schoneveld, P.W. Serruys, N. Bom, Characterization of plaque components and vulnerability with intravascular ultrasound elastography, Phys. Med. Biol. 45 (2000) 1465–1475, doi:10.1088/0031-9155/45/6/305.
[47] T. Wang, T. Pfeiffer, A. Akyildiz, H.M.M. van Beusekom, R. Huber, A.F.W. van der Steen, G. van Soest, Intravascular optical coherence elastography, Biomed. Opt. Express 13 (2022) 5418, doi:10.1364/BOE.470039.
[48] H.H.G. Hansen, R.G.P. Lopata, C.L. de Korte, Noninvasive carotid strain imaging using angular compounding at large beam steered angles: validation in vessel phantoms, IEEE Trans. Med. Imaging 28 (2009) 872–880, doi:10.1109/TMI.2008.2011510.
[49] V.A. Acosta Santamaría, M.F. García, J. Molimard, S. Avril, Characterization of chemoelastic effects in arteries using digital volume correlation and optical coherence tomography, Acta Biomater. 102 (2020) 127–137, doi:10.1016/j.actbio.2019.11.049.
[50] L.A. Davis, S.E. Stewart, C.G. Carsten, B.A. Snyder, M.A. Sutton, S.M. Lessner, Characterization of fracture behavior of human atherosclerotic fibrous caps using a miniature single edge notched tensile test, Acta Biomater. 43 (2016) 101–111, doi:10.1016/j.actbio.2016.07.027.
[51] S. Guvenir Torun, H.M. Torun, H.H.G. Hansen, C.L. de Korte, A.F.W. van der Steen, F.J.H. Gijsen, A.C. Akyildiz, Multicomponent material property characterization of atherosclerotic human carotid arteries through a Bayesian Optimization based inverse finite element approach, J. Mech. Behav. Biomed. Mater. 126 (2022) 104996, doi:10.1016/j.jmbbm.2021.104996.
[52] S. Guvenir Torun, H.M. Torun, H.H.G. Hansen, G. Gandini, I. Berselli, V. Codazzi, C.L. de Korte, A.F.W. van der Steen, F. Migliavacca, C. Chiastra, A.C. Akyildiz, Multicomponent mechanical characterization of atherosclerotic human coronary arteries: an experimental and computational hybrid approach, Front. Physiol. 12 (2021) 1480, doi:10.3389/fphys.2021.733009.